2011 IEEE International Conference on Rehabilitation Robotics
Rehab Week Zurich, ETH Zurich Science City, Switzerland, June 29 - July 1, 2011

# Stochastic Estimation of Human Shoulder Impedance with Robots: An Experimental Design

Kyungbin Park and Pyung Hun Chang
Department of Mechanical Engineering
KAIST
Daejeon, Korea
pkbin98@kaist.ac.kr, phchang@kaist.ac.kr

*Abstract*— **Previous studies assumed the shoulder as a hinge joint during human arm impedance measurement. This is obviously a vast simplification since the shoulder is a complex of several joints with multiple degrees of freedom. In the present work, a practical methodology for more general and realistic estimation of human shoulder impedance is proposed and validated with a spring array. It includes a gravity compensation scheme, which is developed and used for the experiments with a spatial three degrees of freedom PUMA-type robot. The experimental results were accurate and reliable, and thus it has shown a strong potential of the proposed methodology in the estimation of human shoulder impedance.**

***Keywords- stochastic estimation; shoulder; impedance measurement; gravity compensation; impedance control***

## I. INTRODUCTION

This paper concerns itself with the human shoulder impedance measurement by using the combined dynamics of human shoulder and a robot in Fig. 1. More specifically, it proposes a practical methodology to apply the stochastic estimation with internal model based impedance control (IMBIC) to the estimation of human shoulder impedance. Described below are the background and context of the research reported in this paper.

The physical quantity corresponding to clinical assessment of muscle tone-a muscle's resistance to passive elongation or stretch-is mechanical impedance, which characterizes the dynamic relation between motion and force, and may be considered a dynamic generalization of stiffness (i.e., the static relation between displacement and force) [1]-[2]. Reasons for measuring human arm impedance range from understanding basic physiological properties of muscle [3] to testing different hypotheses concerning the maintenance of posture or the control of movement [1], [4]. Behavioral studies have also investigated how human arm impedance properties vary with motor learning [5]. Recently, for the quantitative diagnosis of stroke patients, human arm impedance was measured [2].

For this reason, many research works for the accurate and reliable estimation of human arm impedance have done. Initial studies on measurement of human arm stiffness [3] were extended to the estimation of arm impedance, which includes dynamic parameters such as inertia and viscous damping as well as stiffness, in later studies [6]-[7]. Recently, stochastic estimation methods [2], [8]-[9] have attracted much attention owing to a number of significant advantages over previous methods.

In most previous studies [2] [6]-[7] [10], however, human arm impedance has been estimated only in the horizontal plane, typically with the weight of the arm supported against gravity, with the implicit assumption that both the elbow and shoulder act as hinge joints [8]. This is obviously a vast simplification for the shoulder, which is actually a complex of several different joints with multiple degrees of freedom (DOFs) [8]. It is thus expected that examination of human shoulder impedance under more general and realistic conditions will be a critical step towards understanding the shoulder behavior. Therefore, it is our concern how to estimate the impedance of shoulder more generally and realistically.

Shoulder joint has three principal axes and three DOFs of motion and thus its movements can be described with a three DOF ball and socket joint [11]. Transverse axis is related to flexion/extension; antero-posterior axis to abduction/adduction; vertical axis to internal/external rotation; and long axis can be aligned with any of the above three axes [11]. Therefore, we are going to present a methodology to estimate three DOF human shoulder impedance with a spatial PUMA-type industrial robot. It includes necessary experimental setup and a gravity compensation scheme. IMBIC is used to apply stochastic perturbations to the subject; to gently bring the patient's arm to a test location; and to enable an accurate and reliable stochastic estimation of human shoulder impedance by reducing the effect of nonlinear friction in robot joints. In addition, the analytical stochastic estimation method is used to improve the numerical conditioning of the estimate. The effectiveness of stochastic estimation with IMBIC was verified by our previous experiments [10], in which human arm impedance was estimated with a two DOF SCARA-type industrial robot. In this paper, we will extend the usage of the stochastic estimation with IMBIC to the estimation of human shoulder impedance with a three DOF PUMA-type industrial robot. In order to validate the proposed methodology for the estimation of human shoulder impedance, we will perform the estimation on a spring array similar to the one in [2], [10], the stiffness of which is already known.

This paper is organized as follows. In section 2, we propose a practical methodology for the estimation of human shoulder

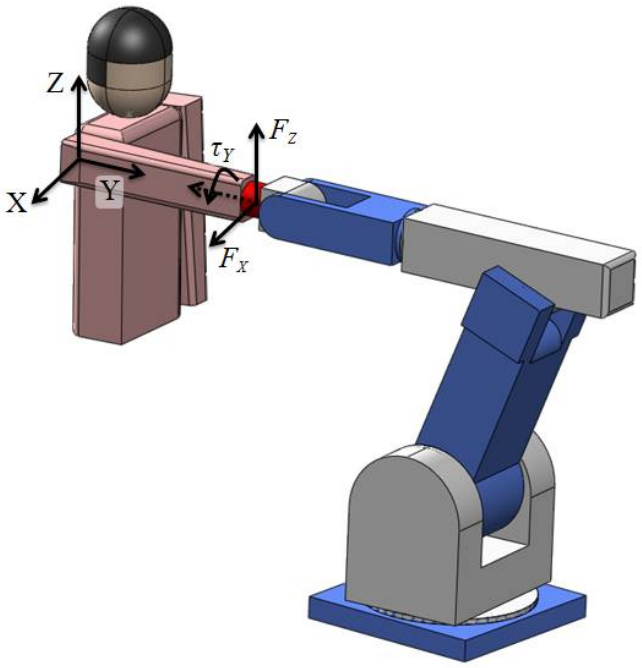


Figure 1. Schematic diagram of robotic estimation of human shoulder impedance. Center of human shoulder joint is set to be the origin of the X, Y, and Z coordinates. Human hand is fixed at and attached to the robot endpoint.

impedance. Section 3 provides the experiments on the spring array. Finally, in section 4, we summarize the results and draw conclusions.

## II. Estimation of Human Shoulder Impedance

### A. Estimation Method

As for the estimation method in the present work, analytical compensation [2], [12]-[13] was used. It is one of the most recent methods and showed good performance in simulations [12] and experiments [2], [10], [13]. During test period for the estimation of human shoulder impedance, the relation among the commanded torque perturbations, $\boldsymbol{\tau}_\Delta$, the interaction torques, $\boldsymbol{\tau}$, and the angular displacement, $\boldsymbol{\theta}$, is depicted using vector and matrix notation as Figs. 2 and 3, similarly to the estimation of human arm impedance [2], [12].

As reported in [2], it is not easy to estimate $\mathbf{C}$ directly from $\boldsymbol{\tau}$ to $\boldsymbol{\theta}$ due to high coherence between the elements of $\boldsymbol{\tau}$. The analytical compensation method resolves this difficulty by analytical compensation for the combined dynamics of human shoulder and robot by using $\hat{\mathbf{R}}$ and $\hat{\mathbf{T}}$ (the estimates of $\mathbf{R}$ and $\mathbf{T}$, respectively) [2], [12]. Consequently, $\hat{\mathbf{C}}$, the estimate of $\mathbf{C}$, can be obtained as follows [2]:

$$\hat{\mathbf{C}} = \hat{\mathbf{R}}\hat{\mathbf{T}}^{-1}, \tag{1}$$

and then $\hat{\mathbf{Z}}$, the estimate of the impedance transfer function matrix (TFM), $\mathbf{Z}$, can be obtained as follows [12]:

$$\hat{\mathbf{Z}} = \hat{\mathbf{C}}^{-1} = (\hat{\mathbf{R}}\hat{\mathbf{T}}^{-1})^{-1} = \hat{\mathbf{T}}\hat{\mathbf{R}}^{-1}. \tag{2}$$

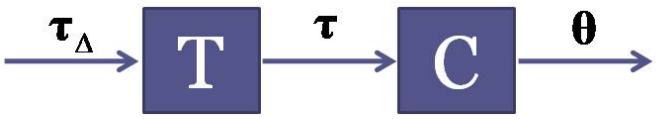


Figure 2. Block daigram of linear MIMO structures using vector and matrix notation: $\mathbf{T}(s)$ is the transfer function matrix from the commanded torque perturbations, $\boldsymbol{\tau}_\Delta$, to the interaction torques, $\boldsymbol{\tau}$; $\mathbf{C}(s)$ from the interaction torques to the angular displacement, $\boldsymbol{\theta}$.


Figure 3. Block diagram of linear MIMO structures using vector and matrix notation: $\mathbf{R}(s)$ is the transfer function matrix from the commanded torque perturbations, $\boldsymbol{\tau}_\Delta$, to the angular displacement, $\boldsymbol{\theta}$.

For the estimation of human shoulder impedance, a subject is seated in front of the robot as shown in Fig. 1. To prevent the estimation results from being affected by the trunk motion, the trunk of the subject is restrained by a seat belt to the chair back. A carbon fiber arm trough is utilized both to prevent wrist and elbow motion and to fix the hand to the handle attached to the robot's end-effector, alleviating the voluntary grasping action that influences the impedance measurements. To avoid voluntary reaction of the subject, the subject is asked to relax his arm. In the estimation of three DOF human shoulder impedance, three-way torque perturbations (in direction of flexion/extension, abduction/adduction, and internal/external rotation) should be implemented. For the torque perturbations in direction of abduction/adduction and flexion/extension, force perturbations in X- and Z-axis direction are applied to the subject's hand and then torque perturbations to the subject's shoulder are computed by using the well-known relationship

$$\boldsymbol{\tau}_\Delta = \mathbf{J}_h{}^T \mathbf{F}_\Delta, \tag{3}$$

where $\boldsymbol{\tau}_\Delta$ denotes the torque perturbation vector at the subject's shoulder; $\mathbf{F}_\Delta$ the vector of force perturbations; $\mathbf{J}_h$ the Jacobian matrix of human arm. The interaction torques in these directions are also computed by using the same relationship with the interaction forces, $\mathbf{F}$, and the angular displacements are calculated by the kinematic relationship between the shoulder rotation and hand's position. As for the direction of internal/external rotation, the torque perturbation, interaction torque, and angular displacement at the subject's hand are assumed to be identical to those at the subject's shoulder.

### B. Gravity Compensation

The gravity force affects the estimation results unless it is properly compensated. In previous studies for the estimation of human arm impedance, lower arm was supported in the horizontal plane by a sling attached to the ceiling to prevent the estimation results from being affected by the gravity force [3], [7]. This method, however, is not appropriate to spatial shoulder impedance measurement with spatial robots. In this paper, thus, we propose a gravity compensation method by

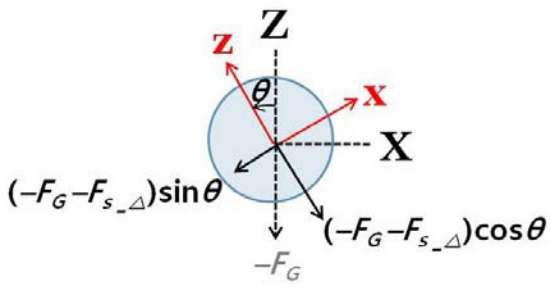


Figure 4. Schematic diagram of F/T sensor and sensed forces. X and Z coordinates are the reference frame; x and z coordinates are the sensor frame.

subtraction gravity force from the sensed values at the force/torque (F/T) sensor.

At the beginning of the test, the sensed value from F/T sensor involves the intrinsic bias error of F/T sensor and gravity force. Note that, for the simplicity, further description is focused on the direction of Z-axis (see Fig. 4).

$$F_{sensed\_z\_i} = -F_G - F_{IBE}, \tag{4}$$

where $F_{sensed\_z\_i}$ denotes the initial sensed value from F/T sensor; $F_G$ gravity force; $F_{IBE}$ the intrinsic bias error. The gravity force is constant on the reference frame (X and Z in Fig. 4), while the intrinsic bias error of F/T sensor is constant on the sensor frame (x and z in Fig. 4). For this reason, the gravity force and the intrinsic bias error should be compensated separately.

***Step 1***. In order to compensate the intrinsic bias error, the robot is posed as shown in Fig. 5(a) prior to the test, and the x- and z-axis sensed values from F/T snesor are stored. Note that the stored values are free from the gravity force. Ten trials are run in succession and the mean value of ten trials is stored as the intrinsic bias error. The intrinsic bias error varies with experimental environment, but it was assumed that the experimental environment is not rapidly changed during the test period and this assumption was justified through ten trials. Hereafter, this stored value will be subtracted from every sensed value at F/T sensor during the test.

***Step 2***. The pose of the robot is changed into test position as shown in Fig. 5(b). Now, F/T sensor values at the beginning of the test include only the gravity force:

$$F_{sensed\_z\_i} = -F_G. \tag{5}$$

This value is transformed relative to the reference frame and stored. In the experimental setup as shown in Fig. 5(b), the transformed value is identical to $F_{sensed\_z\_i}$ in (5) since $\theta$ is zero at the beginning of the test:

$$F_{Z\_i} = -F_G. \tag{6}$$

During the test period, the sensed values after being compensated for the intrinsic bias error are expressed as follows:

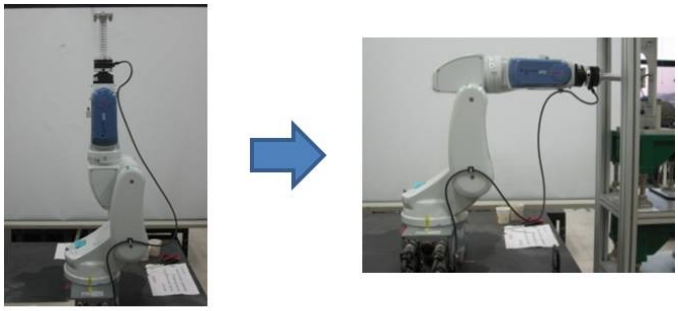


Figure 5. (a) Initial pose of the robot for compensation for the intrinsic bias error of F/T sensor. (b) Robot's pose during the test.

$$\begin{aligned} F_{sensor\_x} &= (-F_G - F_{s\_\Delta})\sin\theta, \\ F_{sensor\_z} &= (-F_G - F_{s\_\Delta})\cos\theta, \end{aligned} \tag{7}$$

where $F_{s\_\Delta}$ denotes the force resulted from subject's impedance, which should be measured for impedance measurement. The transformed values of them relative to the reference frame include both the gravity force and the resultant force from subject's impedance:

$$F_Z = -F_G - F_{s\_\Delta}. \tag{8}$$

The resultant force from subject's impedance is finally acquired by a simple subtraction of (6) from (8):

$$F_Z = -F_{s\_\Delta}. \tag{9}$$

In summary, in order to prevent the estimation results from being affected by the intrinsic bias error and the gravity force, the former is compensated in the sensor frame and the latter on the reference frame.

## III. Validataion via Mechanical Spring Array

### A. Experimental Setup

#### 1) Robot

The robot used in the experiment is a three DOF PUMA-type industrial robot, Samsung Faraman-AT2, as shown in Fig. 5(a) and 5(b). It was used to implement force perturbation X- and Z-axis direction and torque perturbation around Y-axis. The effect of the resultant displacement in Y-axis direction and axis tilt on the estimation was assumed to be negligible since they are much smaller in comparison with the resultant translations in other directions and rotation around Y-axis, respectively. The kinematic information is shown in Fig. 6 and Table I which is expressed by using Denavit-Hartenberg (D-H) parameters in Craig's notation [14]. AC servo motors with the maximum continuous torques of 0.637, 0.319, and 0.319 Nm are used to transmit power through harmonic drives with gear reduction ratios of 120:1, 120:1, and 100:1 for joints 1, 2, and 3, respectively. AC servo drives use torque-controlled mode, and their voltage to torque ratios are calculated by the manufacturer's manual as follows: (25.45, 12.71, 10.62) Nm/V. Each joint has an encoder attached at its shaft for sensing the angular displacement with a resolution of 2048 pulses/rev and

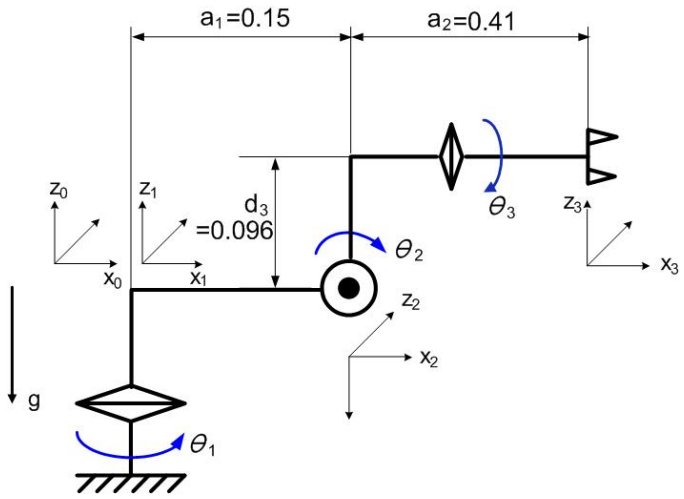


Figure 6. The kinematic information of three DOF PUMA-type industrial robot used in the experiments.

TABLE I. D-H PARAMETERS OF THE ROBOT IN CRAIG'S NOTATION

| $i$ | $\alpha_{i-1}$ | $a_{i-1}$ | $d_i$ | $\theta_i$ |
|---|---|---|---|---|
| 1 | 0 | 0 | 0 | $\theta_1$ |
| 2 | −90° | $a_1$ | 0 | $\theta_2$ |
| 3 | 90°+ $\theta_3$ | $a_2$ | $d_3$ | 0 |

(Units: meter, degree)

thus the resolution of each robot joint is $3.66\times10^{-4}$ deg. (quadrature encoder). The angular velocity and acceleration were computed by numerical differentiation of the angular displacement. For real-time control of robot, the position and velocity of the robot end-effector in the Cartesian coordinates were determined by forward kinematics and the acceleration was computed by numerical differentiation of the velocity. An ATI Gamma SI-130-10 F/T sensor, having ±130 N range and 1/160 N resolution of sensing force and ±10 Nm range and 1/3200 Nm resolution of sensing torque, is attached at the end-effector to measure the interaction forces and torque between the robot and subject. The implementation of the controller was made in Linux-RTAI, a real-time operating system environment, with a sampling frequency of 1 kHz.

*2) Mechanical spring array*

Similar to that of [2], [10], [13], the mechanical spring array largely consists of 4 parts: an inner fixture, an outer fixture, a handle, and springs (Figs. 7 and 8). The inner fixture was bolted to the end of the handle, which was bolted to the F/T sensor on the robot end-effector. The outer fixture was bolted to a pedestal fixed to a shelf.

Eight bolts locate along the perimeter of both the square outer and inner fixture (four bolts at their corners, four bolts at the midpoints of their sides), and thus eight springs could be mounted between bolts on the inner and outer fixtures to generate a variety of stiffness field. In this study, five springs were employed to generate stiffness fields corresponding to two test configurations (***sa1*** to ***sa2*** in Table II). Note that the locations of the spring mounts (bolts) were specified to ensure that the springs would always be in tension during the experiment.

In order to show the accuracy achieved with the proposed method, a linearized model of the mechanical spring array was developed and the expected value of impedance TFM of the mechanical spring array was computed based on this model. For the stiffness matrix K, the nonlinear restoring forces/torque generated by the spring array were derived and then linearized:

$$\mathbf{K}_{sa}=\begin{bmatrix} k_{11} & k_{12} & k_{13} \\ k_{21} & k_{22} & k_{23} \\ k_{31} & k_{32} & k_{33} \end{bmatrix}, \tag{10}$$

$$k_{11}=k_{1a}+k_{1b}+k_{2a}\left(1-\frac{l_{2a}}{l}\right)+k_{2b}\left(1-\frac{l_{2b}}{l}\right)$$
$$+k_{3a}\left(1-\frac{l_{3a}}{2\sqrt{2}l}\right)+k_{3b}\left(1-\frac{l_{3b}}{2\sqrt{2}l}\right)+k_{4a}\left(1-\frac{l_{4a}}{2\sqrt{2}l}\right)+k_{4b}\left(1-\frac{l_{4b}}{2\sqrt{2}l}\right),$$

$$k_{12}=k_{21}=-\frac{k_{3a}l_{3a}}{2\sqrt{2}l}-\frac{k_{3b}l_{3b}}{2\sqrt{2}l}+\frac{k_{4a}l_{4a}}{2\sqrt{2}l}+\frac{k_{4b}l_{4b}}{2\sqrt{2}l},$$

$$k_{13}=k_{31}=(L-l)\left\{\begin{array}{l} -k_{2a}\left(1-\frac{l_{2a}}{l}\right)+k_{2b}\left(1-\frac{l_{2b}}{l}\right)-k_{3a}\left(1-\frac{l_{3a}}{\sqrt{2}l}\right) \\ +k_{3b}\left(1-\frac{l_{3b}}{\sqrt{2}l}\right)+k_{4a}\left(1-\frac{l_{4a}}{\sqrt{2}l}\right)-k_{4b}\left(1-\frac{l_{4b}}{\sqrt{2}l}\right) \end{array}\right\},$$

$$k_{22}=k_{1a}\left(1-\frac{l_{1a}}{l}\right)+k_{1b}\left(1-\frac{l_{1b}}{l}\right)+k_{2a}+k_{2b}$$
$$+k_{3a}\left(1-\frac{l_{3a}}{2\sqrt{2}l}\right)+k_{3b}\left(1-\frac{l_{3b}}{2\sqrt{2}l}\right)+k_{4a}\left(1-\frac{l_{4a}}{2\sqrt{2}l}\right)+k_{4b}\left(1-\frac{l_{4b}}{2\sqrt{2}l}\right),$$

$$k_{23}=k_{32}=(L-l)\left\{\begin{array}{l} -k_{1a}\left(1-\frac{l_{1a}}{l}\right)+k_{1b}\left(1-\frac{l_{1b}}{l}\right)-k_{3a}\left(1-\frac{l_{3a}}{\sqrt{2}l}\right) \\ +k_{3b}\left(1-\frac{l_{3b}}{\sqrt{2}l}\right)-k_{4a}\left(1-\frac{l_{4a}}{\sqrt{2}l}\right)+k_{4b}\left(1-\frac{l_{4b}}{\sqrt{2}l}\right) \end{array}\right\},$$

$$k_{33}=(L-l)L\left\{\begin{array}{l} k_{1a}\left(1-\frac{l_{1a}}{l}\right)+k_{1b}\left(1-\frac{l_{1b}}{l}\right)+k_{2a}\left(1-\frac{l_{2a}}{l}\right)+k_{2b}\left(1-\frac{l_{2b}}{l}\right) \\ +2k_{3a}\left(1-\frac{l_{3a}}{\sqrt{2}l}\right)+2k_{3b}\left(1-\frac{l_{3b}}{\sqrt{2}l}\right) \\ +2k_{4a}\left(1-\frac{l_{4a}}{\sqrt{2}l}\right)+2k_{4b}\left(1-\frac{l_{4b}}{\sqrt{2}l}\right) \end{array}\right\},$$

where $k_i$ and $l_i$ are the nominal stiffness and free length of each spring; $l$ denotes the length from one mounting point on the outer fixture to one on the inner fixture, when they lie on horizontal or vertical line; and $L$ denotes the length between any two adjacent mounting points on the outer fixture of the spring array.

Note that complete pairing of springs (i.e., arrangement of springs to be $k_{ia}=k_{ib}=k_i$ and $l_{ia}=l_{ib}=l_i$ where $i$=1, 2, 3, 4) makes the off-diagonal elements of impedance TFM are numerically ill-conditioned since the inertia and stiffness matrices are isotropic, which causes the spectral estimate to be

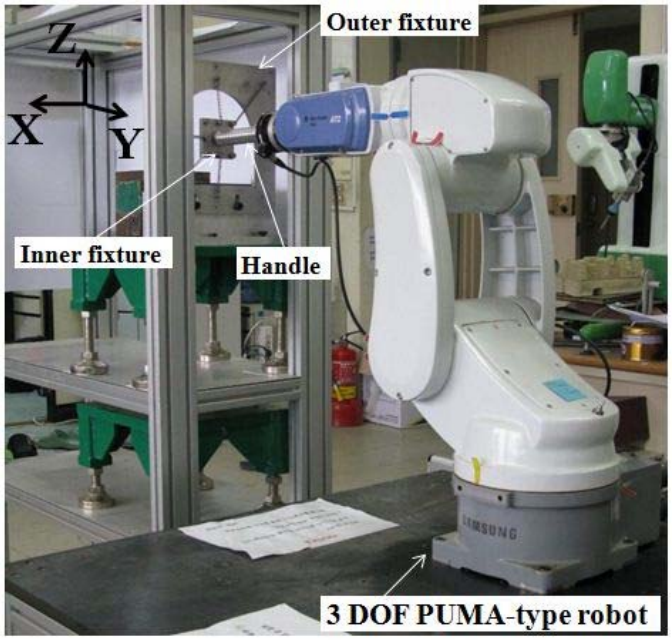


Figure 7. 3 DOF PUMA-type robot and the mechanical spring array used in the experiments. The spring array consists of an inner fixture, an outer fixture, a handle and springs, the stiffness values of which are known in advance.

inaccurate [2], [10]. For fair evaluation of the proposed methodology, the inner and outer fixtures were connected diagonally by springs with different nominal stiffness (i.e., $k_{3a} \neq k_{3b}$ or $k_{4a} \neq k_{4b}$). This arrangement of springs results in the existence of initial restoring forces, which affect the estimation of the impedance TFM. The initial restoring forces are constant on the reference frame the same as the gravity force and measured with the gravity force from F/T sensor at the beginning of the test. The initial restoring forces, therefore, are compensated with the gravity force by *Step 2* in Section 2.B.

In order to reduce numerical errors resulted from handling sparse matrices, centimeter (cm), degree, centinewton (cN) and centinewton centimeter (cNcm) were used to calculate the stiffness matrix as the units of displacement, angular displacement, force, and torque, respectively. The calculated stiffness matrix, which corresponds to $\mathbf{K}_{sa1}$, were given by

$$\mathbf{K}_{sa1} = \begin{bmatrix} 167.5576\,(\text{cN/cm}) & 14.9006\,(\text{cN/cm}) & 2.0424\,(\text{cN/deg.}) \\ 14.9006\,(\text{cN/cm}) & 167.5576\,(\text{cN/cm}) & -2.0424\,(\text{cN/deg.}) \\ 117.0200\,(\text{cNcm/cm}) & -117.0200\,(\text{cNcm/cm}) & 95.7488\,(\text{cNcm/deg.}) \end{bmatrix}.$$

This calculated stiffness matrix was confirmed to be within the ±10% manufacturing tolerances of the mechanical spring constants by quasi-static calibration trials. The mass of the handle and inner fixture was measured on a precision scale to be 0.6028 kg, while the moment of inertia about Y-axis was mathematically calculated to be 3.4492 kg·cm$^2$. The diagonal elements of viscous damping matrix were defined such that the damping coefficient $\zeta$ was equal to 0.01, whereas the off-diagonal elements were set to be zero as in [2], [10], [13].

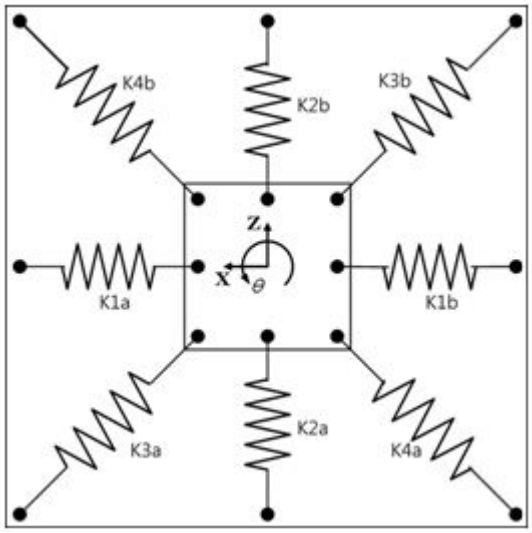


Figure 8. Schematic diagram of the mechanical spring array. Eight springs could be mounted between bolts on the inner and outer fixtures to generate a variety of stiffness field.

TABLE II. SPRING ARRAY TEST CONFIGURATIONS AND STIFFNESS VALUES USED DURING THE SPRING ARRAY IMPEDANCE EXPERIMENTS

| ***Configuration #*** **(N/m)** | **K1a** | **K2a** | **K3a** | **K4a** |
|---|---|---|---|---|
| | **K1b** | **K2b** | **K3b** | **K4b** |
| ***sa1*** | 38.0615 | 38.0615 | 0.0 | 0.0 |
| | 38.0615 | 38.0615 | 0.0 | 66.3707 |
| ***sa2*** | 38.0615 | 38.0615 | 0.0 | 66.3707 |
| | 38.0615 | 38.0615 | 0.0 | 0.0 |

### *B. Desired Impedance and Gains of IMBIC*

IMBIC used in the experiments has the following form [15]-[16]:

$$\mathbf{F}_u(t) = \bar{\mathbf{M}}_x \mathbf{u}(t) + \underbrace{\mathbf{F}_u(t-L) - \bar{\mathbf{M}}_x \ddot{\mathbf{x}}_r(t-L)}_{\text{time delayed estimation (TDE)}}, \quad (11)$$

where

$$\mathbf{u}(t) = \mathbf{v}(t) - \mathbf{M}_{rd}^{-1}(\mathbf{B}_{rd}\dot{\mathbf{x}}_r(t) + \mathbf{K}_{rd}\mathbf{x}_r(t)), \quad (12)$$

with

$$\mathbf{v}(t) = \mathbf{M}_{rd}^{-1}(\mathbf{K}_d \mathbf{x}_{rd} - \mathbf{F}_{sa}(t) + \mathbf{F}_\Delta(t)) + \boldsymbol{\Gamma}\begin{Bmatrix} -[\ddot{\mathbf{x}}_r(t-L) + \mathbf{M}_{rd}^{-1}(\mathbf{B}_{rd}\dot{\mathbf{x}}_r(t-L) + \mathbf{K}_{rd}\mathbf{x}_r(t-L))] \\ +\mathbf{v}(t-L) \end{Bmatrix}, \quad (13)$$

$\mathbf{F}_u = \begin{bmatrix} F_X & F_Z & \tau_Y \end{bmatrix}^T \in \Re^3$ denotes the generalized input force vector at the robot end-effector; $\bar{\mathbf{M}}_x \in \Re^3$ the matrix representing the known part of the robot inertia matrix, $\mathbf{M}_x \in \Re^3$; $\mathbf{x}_r = \begin{bmatrix} X & Z & \theta \end{bmatrix}^T$, $\dot{\mathbf{x}}_r$, $\ddot{\mathbf{x}}_r$ the vectors of position, velocity, and acceleration; $L$ the small time delay; $\mathbf{M}_{rd}$, $\mathbf{B}_{rd}$, $\mathbf{K}_{rd}$ the desired mass, damping and stiffness matrices of the

TABLE III. SPECTRAL ANALYSIS PARAMETERS USED IN SPRING ARRAY IMPEDANCE ESTIMATION EXPERIMENT

| $N_{FFT}$ | $N_{WND}$ | $N_{OVL}$ | $f_r$ [Hz] |
|---|---|---|---|
| 24576 | 24576 | 18432 | 0.041 |

$N_{FFT}$ number of data points included in the FFT calculation; $N_{WND}$ the length of the Hanning window function; $N_{OVL}$ the number of overlapping samples; $f_r$ minimum resolvable frequency.

desired linear model, respectively; $\mathbf{F}_{sa}$ the generalized force applied to the spring array by the robot; $\mathbf{F}_{\Delta}$ stochastic perturbations; and $\mathbf{\Gamma}$ denotes a diagonal forgetting factor matrix whose diagonal elements $\gamma_{ii}$ ($i$=1, 2, 3) lie between zero and one: $0 < \gamma_{ii} < 1$, by which the accumulation of quantization error due to the resolution limit is prevented.

The $\bar{\mathbf{M}}_x$ is determined by the relation [15]-[16]:

$$\bar{\mathbf{M}}_x = \mathbf{J}^{-T}\bar{\mathbf{M}}_\phi\mathbf{J}^{-1}, \tag{14}$$

where $\bar{\mathbf{M}}_\phi$ represents the known part of the joint space robot inertia matrix and $\mathbf{J}$ denotes the Jacobian matrix.

The following gains are used for IMBIC:

$$\mathbf{M}_{rd} = diag(1.0\,\text{kg},\ 1.0\,\text{kg},\ 1.0\,\text{kg}\cdot\text{m}^2),$$
$$\mathbf{B}_{rd} = diag(40\,\text{N}\cdot\text{s/m},\ 60\,\text{N}\cdot\text{s/m},\ 20\,\text{Nm}\cdot\text{s/rad}),$$
$$\mathbf{K}_{rd} = diag(100\,\text{N/m},\ 100\,\text{N/m},\ 100\,\text{Nm/rad}),$$
$$\bar{\mathbf{M}}_\phi = diag(0.00713,\ 0.00614,\ 0.00835),$$
$$\mathbf{\Gamma} = diag(0.9,\ 0.81,\ 0.9).$$

Over damped and critically damped impedance dynamics were selected for displacement and rotation of the robot end point, respectively, while the value of $\bar{\mathbf{M}}_\phi$ and $\mathbf{\Gamma}$ were tuned according to the guideline in [17].

### C. Force/Torque Perturbations

Random force/torque perturbations having low input coherence (less than 0.6 in the frequency range of interest), were generated at a sampling rate of 1000 Hz by filtering a set of uniformly distributed random signals with an eighth-order Butterworth low pass filter having a cut-off frequency 15 Hz (selected to exceed human arm natural frequency, ~2-3 Hz). It is identical to the method of [2], [10]. Peak magnitudes of the resultant interaction force/torque were approximately 4.5 N and 0.1 Nm, respectively.

### D. Estimation by analytical compensation method

The impedance TFM of the spring array was estimated in accordance with the analytical compensation method described in Section 2.A. During test period, force/torque perturbations, $\mathbf{F}_{\Delta sa}$ ($F_{\Delta X}$, $F_{\Delta Z}$ and $\tau_{\Delta Y}$), were generated randomly and stored at the same time. As we were applying the stochastic perturbations, both the inner fixture position, $\mathbf{x}_{sa}$ ($X$, $Z$ and $\theta$), and the interaction force/torque, $\mathbf{F}_{sa}$ ($F_X$, $F_Z$ and $\tau_Y$), between the robot and spring array were measured. The inner fixture position was measured being assumed that the inner fixture was perfectly fixed to the robot end-effector through the handle. The interaction force/torque, on the other hand, was measured by using the F/T sensor attached at end-effecotr. Note that in the estimation of mechanical spring array impedance, force and displacement in X- and Z-axis direction are not necessary to be transformed into torque and angular displacement, which is needed for the estimation of human shoulder impedance.

From the saved $\mathbf{F}_{\Delta sa}$, $\mathbf{x}_{sa}$ and $\mathbf{F}_{sa}$, we firstly estimated $\hat{\mathbf{R}}$ (estimate of TFM from $\mathbf{F}_{\Delta sa}$ to $\mathbf{x}_{sa}$) and $\hat{\mathbf{T}}$ (estimate of TFM from $\mathbf{F}_{\Delta sa}$ to $\mathbf{F}_{sa}$) by using the frequency domain stochastic estimation method [2], [8], [10], [12], [18], and then the impedance TFM of the spring array was finally determined according to (2).

Trials lasted for 50s (50,001 data points), allowing a number of sequential epochs of data to be averaged to reduce random error while allowing an acceptable spectral resolution. Welch's periodogram method was used for the spectral analysis [2], [10], [12], [18]. The parameters in Table III were used, which yielded the best estimation, among many parameter sets tried.

### E. Evaluation method

The reliability and accuracy of the mechanical spring array impedance estimation were evaluated by coherence functions [18]-[19] and two measures defined in [12].

In order to evaluate the reliability of the estimation method, both multiple and partial coherence functions [13], [18]-[19] have been used. Multiple coherence functions, on one hand, indicate how well a given output can be linearly predicted from all of the system inputs and over which frequencies a linear model can accurately characterize the system dynamics. Regions of low multiple coherence indicate insufficient input power, significant system nonlinearities, noise, or contributions from unmeasured inputs [2], [8], [12], [18]. A partial coherence function, on the other hand, measures the linear dependency between one input and a particular output, and is equivalent to ordinary coherence after the effect of the other input has been removed [2], [4], [8], [18].

As for the two measures mentioned above, $\varphi_T$ and $\varphi_{ij}$, have been used to evaluate the accuracy of the estimation method [12]. More specifically, $\varphi_T$ and $\varphi_{ij}$ deal with magnitude and phase errors between expected impedance TFM $\mathbf{Z}_{sa}(s)$ and estimated impedance TFM $\hat{\mathbf{Z}}_{sa}(s)$ without dimensional inconsistency. $\varphi_T$ is defined as the arithmetic mean value of $\Delta Z_{sa}(f_k)$, the difference between $\mathbf{Z}_{sa}(s)$ and $\hat{\mathbf{Z}}_{sa}(s)$ at frequency $f_k$,

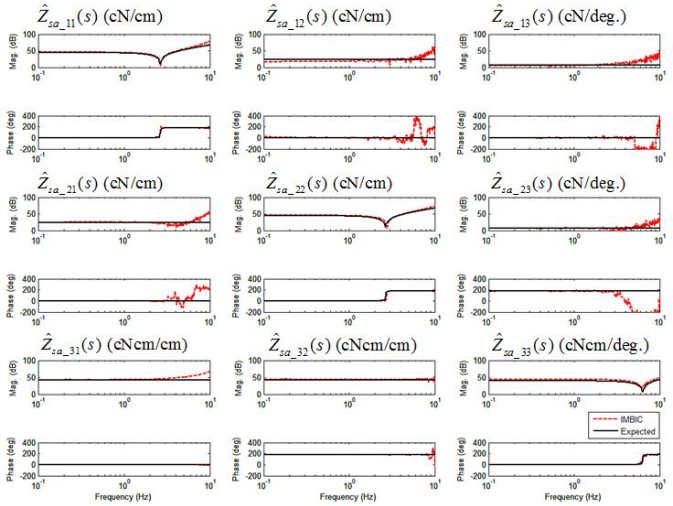


Figure 9. Expected behavior (based on a linearized model) and estimated spring array impedance TFMs with IMBIC. Both magnitude and phase estimation well agree with the expected values throughout the frequency range of interest.

$$\Delta Z_{sa}(f_k) \triangleq \left\| \mathbf{Z}_{sa}(j2\pi f_k) - \hat{\mathbf{Z}}_{sa}(j2\pi f_k) \right\|_2, \quad f_k \in [0 \ f_{\max}] Hz, \tag{15}$$

where $f_{\max}$ denotes the maximum frequency of interest; and $\|\mathbf{G}\|_2$ denotes the regular Euclidean norm of the complex matrix $\mathbf{G}$ and is equal to the maximum singular value of $\mathbf{G}$ [20]. In this study, $f_{\max}$ is set to be 10Hz, which is more than three times the natural frequency of human arm. Similarly, $\varphi_{ij}$ ($i, j$=1, 2, 3) was defined as the mean value of $\Delta Z_{sa\_ij}(f_k)$, the difference between the $i, j$-th element of $\mathbf{Z}_{sa}$ and $\hat{\mathbf{Z}}_{sa}$ at frequency $f_k$,

$$\Delta Z_{sa\_ij}(f_k) \triangleq \left| Z_{sa\_ij}(j2\pi f_k) - \hat{Z}_{sa\_ij}(j2\pi f_k) \right|, \quad f_k \in [0 \ f_{\max}] Hz. \tag{16}$$

In accordance with their definition, $\varphi_T$ represents the whole accuracy of $\hat{\mathbf{Z}}_{sa}$, whereas $\varphi_{ij}$ stands for the individual accuracy of $i, j$-th element of $\hat{\mathbf{Z}}_{sa}$. Zero value of $\varphi_T$ and $\varphi_{ij}$ indicates that the estimated impedance TFM $\hat{\mathbf{Z}}_{sa}(s)$ is identical to the expected value of mechanical spring array's impedance TFM $\mathbf{Z}_{sa}(s)$ [12].

### F. Experimental Results

For each of the two test configuration, ***sa1*** to ***sa2***, six trials were run in succession and then the respective mean of estimated mechanical spring array impedance TFMs of six trials was obtained. Of the two, the estimated impedance for ***sa1*** is shown in Fig. 9 and the corresponding coherence functions are shown in Fig. 10. In Figs. 9 and 10, dashed line indicates the spectral estimates and coherence functions under the IMBIC, while, in Fig. 9, the expected behavior from the linear model is depicted by solid line. Fig. 11, on the other hand, displays the accuracy measures ($\varphi_T$ and $\varphi_{ij}$) for all the two configurations.

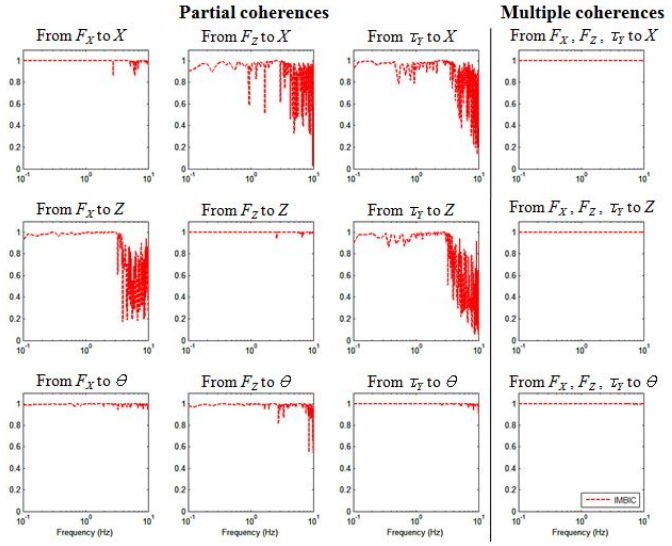


Figure 10. Partial and multiple coherence functions that correspond to the estimates shown in Fig. 9. All coherence functions are close to unity throughout the frequency range of interest.

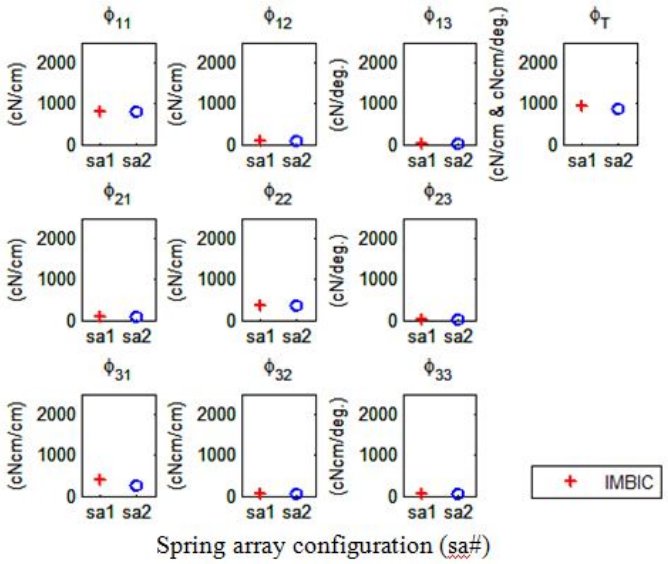


Figure 11. Summary of estimation accuracy of each element, $\varphi_{ij}$, and that of the entire TFM, $\varphi_T$, for all two test configurations *sa1* to *sa2*.

Figs. 9 and 11 show excellent agreement between the estimated and expected impedance matrix, in terms of both the magnitudes and phases of all its elements. In Fig. 10, all the partial and multiple coherence functions have values significantly close to unity. Especially, it is noticeable that the multiple coherence function values exceed 0.95 throughout the frequency range of interest.

### G. Discussion

High multiple coherence function values mean that the estimated impedance TFM accurately characterizes the mechanical spring array dynamics, and thus that the estimation results are reliable.

The estimated spring array impedance TFMs well agree with the expected values throughout the frequency range of interest except for the estimated phase of some of its off-diagonal elements ($f$ > 5 Hz). Above 5 Hz, some of the estimated impedance begin to deviate from second-order behavior. However, in this case the partial coherences also are low and fluctuating, showing the sensitivity of the stochastic estimation. The accuracy measures have values in the same order as in the estimation of human arm impedance simulation [12] and experiments [10]. The above indicates that the estimation results are accurate.

## IV. CONCLUSION

The research in this article began with a question, *"How to estimate the impedance of shoulder more generally and realistically?"* We have proposed a practical methodology, which involves necessary experimental setup and gravity compensation scheme, for applying the stochastic estimation with IMBIC to the estimation of human shoulder impedance with a spatial robot. The estimation results were accurate and reliable, providing an affirmative answer. Having proposed a practical method and verified its effectiveness by experiments on a mechanical system, spatial human shoulder impedance estimation will be the next step and is currently underway.

## ACKNOWLEDGMENT

This work was supported by Technology Innovation Program (Innovation Cluster Program) through the Korea Innovation Cluster Foundation funded by the Ministry of Knowledge Economy (MKE, Korea) (No. 1415113260).

## REFERENCES

[1] N. Hogan, "Skeletal muscle impedance in the control of motor actions," J. Mech. Med. Biol., vol. 2, pp. 359-373, June 2002.

[2] J. J. Palazzolo, et al., "Stochastic estimation of arm mechanical impedance during robotic stroke rehabilitation," IEEE Trans Neural Syst Rehabil Eng, vol. 15, pp. 94-103, 2007.

[3] F. Mussa-Ivaldi, N. Hogan, and E. Bizzi., "Neural, mechanical, and geometric factors subserving arm posture in humans," J. Neurosci., vol. 5, pp. 2732-2743, October 1, 1985.

[4] H. Gomi and M. Kawato, "Human arm stiffness and equilibrium-point trajectory during multi-joint movement," Biol Cybern, vol. 76, pp. 163-171, 1997.

[5] E. Burdet, R. Osu, D. W. Franklin, T. E. Milner, and M. Kawato, "The central nervous system stabilizes unstable dynamics by learning optimal impedance," Nature, vol. 414, pp. 446-449, 2001.

[6] J. M. Dolan, M. B. Friedman, and M. L. Nagurka., "Dynamic and loaded impedance components in the maintenance of human arm posture," IEEE Trans Syst Man Cybern, vol. 23, pp. 698-709, 1993.

[7] T. Tsuji, P. G. Morasso, K. Goto, and K. Ito, "Human hand impedance characteristics during maintained posture," Biol Cybern, vol. 72, pp. 475-485, 1995.

[8] E. J. Perreault, R. F. Kirsch, and A. M. Acosta, "Multiple-input, multiple-output system identification for characterization of limb stiffness dynamics," Biol Cybern, vol. 80, pp. 327-337, 1999.

[9] E. de Vlugt, A. C. Schouten, and F. van der Helm, "Closed-loop multivariable system identification for the characterization of the dynamic arm compliance using continuous force disturbances: a model study," J Neurosci Methods, vol. 122, pp. 123-140, 2003.

[10] P. H. Chang, K. Park, S. H. Kang, H. I. Krebs, and N. Hogan, "An experimental stochastic estimation of human arm impedance with robots having nonlinear frictions," unpublished.

[11] H. C. Kwon and H. S. Kim, Musculoskeletal Examination, Jungmunkag, 1998.

[12] P. H. Chang and S. H. Kang, "Stochastic estimation of human arm impedance under nonlinear friction in robot joints: A model study," J Neurosci Methods, vol. 189, pp. 97-112, 2010.

[13] J. Palazzolo, "Robotic technology to aid and assess recovery and learning in stroke patients," Ph.D thesis, Dept. Mech. Eng., Massachusetts Institute of Technology, Cambridge, 2005.

[14] John J. Craig, "Introduction to Robotics: Mechanics and Control," 3rd ed., Prentice Hall, 2005.

[15] S. H. Kang, Jin M, and P. H. Chang, "An IMC based enhancement of accuracy and robustness of impedance control," in Proceedings of the IEEE Conference on Robot Autom, Pasadena, CA, 2008, pp. 2623-2628.

[16] S. H. Kang, Jin M, and P. H. Chang, "A Solution to the accuracy/robustness dilemma in impedance control," IEEE/ASME Trans Mechatronics, vol. 14, pp. 282-294, 2009.

[17] S. H. Kang, "Robust IMC based impedance control of robot manipulator," Ph.D thesis, Dept. Mech. Eng., KAIST, 2009.

[18] J. S. Bendat and A. G. Piersol, Random Data: Analysis and Measurement Procedures, 2nd ed. New York: Wiley, 1986.

[19] R. J. Patton, M. Miles, and P. Taylor, "Use of the coherence function for a comparison of test signals for frequency domain identification," in Proceedings of the IEEE international conference on control, Edinburg, UK, 1991, pp. 651-657 vol.1.

[20] H. K. Khalil, "Nonlinear Systems," 3rd ed Upper saddle River, NJ: Prentice Hall, 2002, p. 210.